Structural Changes of the W(211) Surface Induced by Ultrathin Films of Rh, Pt, and Pd†

Kalman Pelhos,‡ Ihab M. Abdelrehim,§ Cheng-Hsun Nien,|| and Theodore E. Madey*

Department of Physics and Astronomy and Laboratory for Surface Modification, Rutgers, The State University of New Jersey, Piscataway, New Jersey 08854-8019

Received: August 1, 2000; In Final Form: December 24, 2000

A W(211) surface covered with a thin film (between 0.5 and 1 physical monolayer) of Rh, Pt, or Pd is found to exhibit an $n \times 1$ superstructure when annealed above a threshold temperature of ~900 K (500 K for Pd). The superstructure is observed using low energy electron diffraction; phase diagrams are presented to indicate the coverage range and the temperature threshold where the new structure appears. Scanning tunneling microscopy results indicate that in the case of Pd/W(211) the superstructure phase is due to missing overlayer rows. In the case of Rh/W(211), there are two possible interpretations to the observed periodic structure: either the adlayer forms an ordered superstructure or the W surface itself forms a microfaceted structure with {110} faces. On the basis of our STM observations of gas adsorption on the surface, we found the explanation involving microfacets more plausible. A careful calibration of overlayer coverage is performed using a quartz crystal monitor combined with temperature programmed desorption measurements performed at high temperatures (up to 2400 K). Auger electron spectroscopy used in combination with thermal annealing series demonstrates that overlayer coverages above one physical monolayer are thermally unstable, which is explained by the formation of an ultrathin alloy film.

I. Introduction

Bimetallic systems, consisting of metal films deposited onto crystalline metal substrates, are of great interest to surface scientists because they provide model catalytic systems for investigating a wide range of physical and chemical processes under highly controlled experimental conditions. A wide variety of surface/interface phenomena have been observed when growing thin metallic films on metal surfaces, including, for example, surface reconstruction,[1−7] (sub)surface alloy formation,[8,9] faceting,[10−12] the formation of clusters[13−15] or other superstructures,[16,17] and cluster encapsulation.[18,19] Changes in the geometrical[12,20−22] and/or electronic structure[23−27] of the overlayer as a function of film thickness have also been observed. Our group has focused on studying a special class of bimetallic systems: ultrathin metal films, up to a few atomic layers thick, on atomically rough metal surfaces, for example bcc(111). A special emphasis is placed on the structural investigation of these surfaces, because they are found to undergo massive morphological restructuring under certain conditions.

Specifically, we have recently studied the faceting of the W(111) and Mo(111) surfaces as induced by ultrathin films of Pt, Pd, Au, Rh, and Ir.[28−30] These metal-covered bcc(111) surfaces are found, upon high-temperature annealing, to form large scale pyramids (up to a thousand angstroms in size) with faces of {211} orientations as evidenced by both low energy electron diffraction (LEED) and scanning tunneling microscopy (STM). These observations are consistent with early LEED observations that gaseous adsorbates cause faceting of W(111) and Mo(111).[31−34] The driving force behind the metal film induced morphological change is understood to be the reduction of the total surface free energy, as supported by theoretical calculations that use either embedded atom methods[35] or a first principles approach.[36] In more general terms, the faceting is caused by the large anisotropy of the surface free energy γ for the adsorbate-covered bcc metal.

LEED observations suggest, however, that under special circumstances the (211) faces of these pyramids may undergo further restructuring,[37] which encouraged us to investigate these surfaces in detail. In addition, W(211) has been observed, using LEED, to undergo $n \times 1$ type surface reconstruction after adsorption of oxygen and annealing.[31,38] There are also reports in the literature of $n \times 1$ type surface reconstructions of various *clean* fcc(110) surfaces (they are similar to bcc(211) surfaces in their row-and-trough structure) via the formation of microfacets.[39−45] In this paper, we report on our investigation of the surface reconstruction of W(211) induced by ultrathin metal films of Rh, Pt, and Pd. These three metals are chosen because they all cause faceting of the W(111) surface. Moreover Pt and Rh monolayers have very high desorption temperatures (above ~1500 K); therefore, the Pt/W and Rh/W systems can be annealed to very high temperatures without loss of material. The Pt/W and Pd/W systems show interesting chemical properties as bimetallic catalysts. Our group has studied catalytic *n*-butane hydrogenation on Pt/W[46] and acetylene cyclotrimerization to benzene on Pd/W[47,48] as well as the sensitivity of both reactions to surface structure.

II. Experimental Section

All experiments have been performed in one of two stainless steel ultrahigh vacuum (UHV) systems. The first, that we refer to as the "reaction" chamber, has an average base pressure below

† Part of the special issue "John T. Yates, Jr. Festschrift".

* To whom correspondence should be addressed. E-mail: madey@physics.rutgers.edu.

‡ Present address: Agere Systems, 600 Mountain Avenue, Murray Hill, NJ 07974.

§ Present address: National Semiconductor Corporation, 5 Foden Road, South Portland, ME 04106.

|| Present address: Institute of Physics, Academia Sinica, Nankang, Taipei, Taiwan 11529.

10.1021/jp0027501 CCC: $20.00
Published on Web 04/03/2001

1×10^{-10} Torr; it is equipped with a double pass cylindrical mirror analyzer and a grazing incidence electron gun for Auger electron spectroscopy (AES), a four grid LEED optics, a quadrupole mass spectrometer (QMS), and a quartz crystal monitor (QCM).

The sample used in the reaction chamber is a W single-crystal disk (approximately 1 mm thick and 1 cm in diameter) oriented and mirror-polished to within 0.5° of the (211) plane. The sample holding assembly is specially designed to achieve a wide temperature range (100−2500 K) while minimizing both outgassing during TPD experiments and cooling times afterward. The sample is supported by a Ta wire (0.5 mm diameter) loop, spot-welded to the circumference of the sample at several points; this Ta wire is also used for heating the sample to lower temperatures (<1500 K) by passing high currents (up to 25 A) through the loop. The sample may be cooled to 100 K using liquid-nitrogen cooling. To achieve high temperatures (up to 2500 K), a spiral W filament is mounted directly behind the sample for electron bombardment heating; the sample is kept at a high positive potential (1500 V), and at maximum temperatures, the emission current from the spiral W filament reaches 200 mA. The temperature of the sample is measured by a W-5%Re—W-26%Re thermocouple that is spot-welded to the backside of the sample. The sample is cleaned by heating in 10^{-7} Torr oxygen at 1000 K to oxidize carbon contamination, followed by a rapid flash to 2400 K to desorb oxygen from the surface. Also, all metals studied can be removed from the surface completely by high-temperature treatment.

Ultrathin metal films are deposited from one of three metal evaporators; two may be cooled by water or liquid nitrogen. A movable quartz crystal microbalance (QCM) may be positioned in front of them for absolute calibration of the metal flux; when dosing the sample, the QCM is moved out of the way. The third evaporator is located directly opposite the mass spectrometer, enabling us to observe the dosed species directly. Each overlayer metal has been deposited from both types of evaporators to ensure consistency of the data.

The Pt evaporator consists of a piece of high purity Pt foil (0.1 mm thick, 1 × 4 mm in size) spot-welded to a W wire (0.5 mm in diameter); the Rh and Pd sources are 0.125 mm diameter high purity wire wrapped around a 0.5 mm tungsten wire in a coil of ∼5 mm length. The tungsten wire is heated resistively to cause the evaporation (sublimation) of Pt, Rh, or Pd. Outgassing loops enable a thorough degassing of the source without loss of material, and the pressure in the chamber remains below 2×10^{-10} Torr even while dosing Pt at a source temperature of ∼1700 K. To minimize sample contamination during overlayer deposition, evaporation rates on the order of one physical monolayer per 10 minutes are used. Using the evaporator that is directly facing the mass spectrometer, we find that when evaporating Pt and Rh at very high temperatures W may be co-deposited with these metals (from the hot W wire) but only in negligible quantities (<0.5%).

Although QCM data provide an absolute measure of overlayer coverage, subsequent relative coverage measurements are made using temperature programmed desorption (TPD) and/or overlayer-to-substrate peak intensity ratios in AES spectra. In a typical TPD run, the sample is heated by electron bombardment at a rate of 10 K/s to temperatures as high as 2400 K. Using a computer to control the current in the spiral W filament during TPD experiments, a 10 K/s linear temperature ramp may be achieved with less than ±2 K deviation from the desired temperature.

The thermal stability of overlayer films is investigated by measuring Auger annealing curves (i.e., plots of Auger signal intensity vs sample annealing temperatures).[49] After metal deposition, the sample is annealed for two minutes at a given temperature in a sequence of increasing temperatures ranging from 400 K until the metal film is desorbed (1900 K for Pt and Rh, 1500 K for Pd). After each two-minute annealing, the sample is cooled to room temperature and Auger spectra are obtained.

The same sequence of annealing experiments is repeated to study structural changes of the surface with increasing temperature using LEED. The LEED observations are made after each annealing step at room temperature, with electron energies between 50 and 250 eV. Results are recorded using a single lens reflex camera, fast (ISO1000) film, and long exposure times (0.5 to 3 min).

STM measurements are performed in the second vacuum chamber that has a base pressure below 2×10^{-10} Torr; it houses a McAllister UHV scanning tunneling microscope, a single pass cylindrical mirror analyzer with a concentric electron gun, and a four grid rear-view LEED optics. The same W(211) sample as above is supported by a Ta wire (0.5 mm diameter) loop; the Ta loop is spot-welded to a molybdenum cylinder that serves as the structural support during STM scans. Ultrathin Pt, Pd, or Rh films are deposited from water-cooled metal evaporators similar to the ones in the reaction chamber.

In the STM chamber, the sample may be positioned in front of a spiral W filament for electron beam heating, which is used to clean the sample of surface contaminants by flashing the surface to high temperatures (up to 2300 K). A second spiral W filament is part of the sample holder and is normally situated behind the sample, inside the molybdenum support cylinder (except while scanning). This second filament is used for e-beam heating when annealing the sample at "low" temperatures (up to 1400 K). With the heating filament mounted behind the sample, we are able to use an infrared pyrometer to measure the temperature during annealing at temperatures above ∼800 K.

In a typical STM experiment, the surface is cleaned, after which its cleanliness is verified by AES. The clean sample is covered with a thin film of Pt, Pd, or Rh; then, an AES spectrum is obtained. The overlayer-to-substrate Auger peak intensity ratio can be used to estimate the coverage, on the basis of QCM and AES measurements performed in the reaction chamber. The overlayer covered sample is annealed to a set temperature between ∼700 and 1400 K; the annealing time is usually one minute but may be as long as 10 minutes for some experiments. After the sample is allowed to cool to room temperature, another AES spectrum is obtained. Reconstructed surface structures are identified using LEED, and finally, the sample is transferred to the STM for scanning.

III. Results

As discussed below, LEED observations show that the W(211) surface, when covered with a thin film of Pt, Pd, or Rh, may form an $n \times 1$ type superstructure upon annealing. In either case, it is found that the superstructure phase is limited to a very narrow coverage range; therefore, it is essential to establish reliable coverages for the thin films in question. Consequently, we begin by discussing the results of a combination of QCM and TPD measurements aimed at determining the overlayer coverage. Second, we present results from Auger annealing curves, which provide information on the thermal stability of the overlayer films and further (indirect) evidence

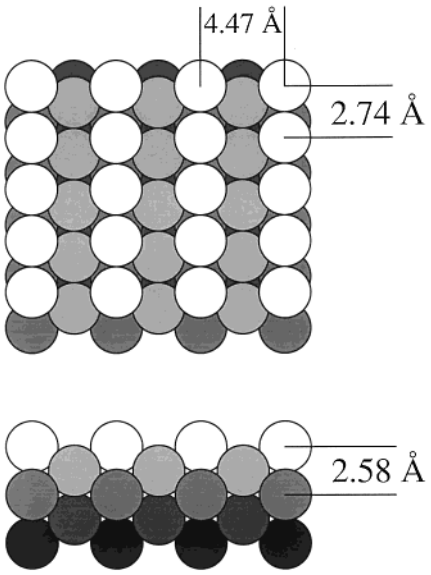

Figure 1. Ball model of W(211) surface. The row and trough structure runs parallel to the closed packed [$\bar{1}$11] direction

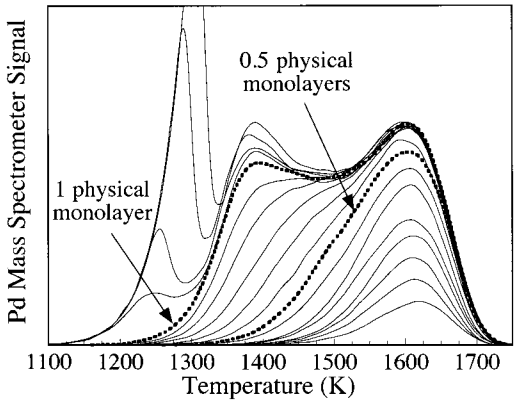

Figure 2. Temperature programmed desorption of Pd from W(211). Coverages of one-half and one full physical monolayer are indicated in bold dashed lines, as measured by a QCM.

on the overlayer coverage. Third, we present phase diagrams (surface structure vs overlayer coverage and annealing temperature) based on LEED observations. Finally, we discuss the real-space structure of the observed superstructures based on STM measurements.

III.a. Measurement of Coverage. We define one *physical* monolayer on the W(211) surface as the overlayer coverage where every W atom normally exposed to the surface is covered by an adsorbate atom; this corresponds to an absolute coverage of 1.63×10^{15} atoms/cm^2. Note that, because of the atomic scale roughness of the W(211) surface (Figure 1 shows its row and trough structure), a coverage of one physical monolayer includes two *geometrical* monolayers, where adatoms in the first geometrical monolayer are adsorbed in the troughs, whereas the second geometrical monolayer covers the topmost row of tungsten atoms.

TPD spectra have been obtained for all three metal overlayers with coverages ranging from approximately 0.1 up to a few physical monolayers. Pd/W(211) TPD spectra in Figure 2 display three desorption peaks. The coverage that corresponds to the saturation of the highest temperature peak ($T_p \sim 1610$ K) has been calibrated against QCM measurements several times. These measurements all indicate, within a 10% uncertainty, an absolute coverage of 0.5 physical monolayers; Pd

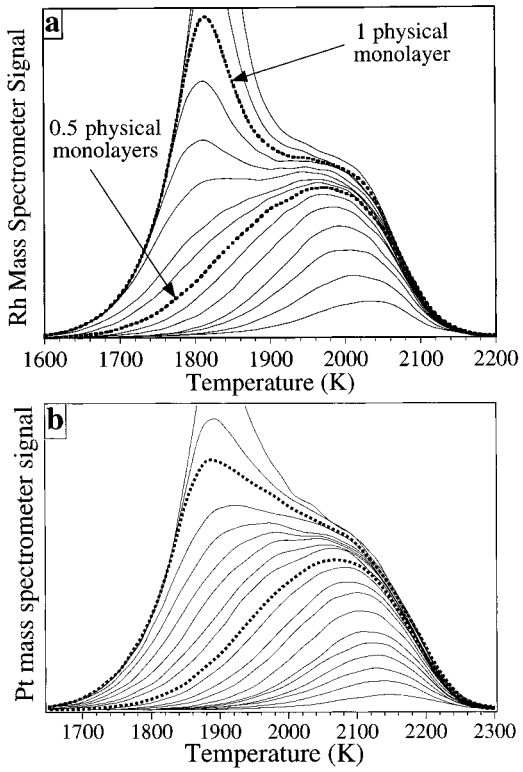

Figure 3. Temperature programmed desorption of Rh (a) and Pt (b) from W(211). Coverages of one-half and one full physical monolayer are indicated in bold dashed lines.

atoms are believed to cover the troughs of the W(211) surface leaving W atoms in the rows exposed. The middle peak ($T_p \sim$ 1390 K) corresponds to the second half physical monolayer, which covers the remaining exposed W atoms. The saturation of these two higher temperature peaks together corresponds to one physical monolayer Pd coverage. The third and lowest temperature ($T_p < 1300$ K) peak in the TPD spectra is attributed to Pd in excess of one monolayer (so-called "multilayer" peak). In the Pt or Rh TPD spectra (Figure 3), we observe only two distinct desorption peaks. In both cases, QCM measurements confirm that the high-temperature peak is related to the first half physical monolayer, whereas the second half-monolayer peak overlaps with the multilayer peak, and they cannot be resolved. Special coverages of 0.5 and 1 physical monolayers are indicated in bold dashed lines on each TPD spectrum.

TPD spectra are very accurate tools for coverage measurement (when calibrated against the QCM); by calculating the integrated area under a desorption curve, the coverage can be determined with 5% absolute accuracy (essentially the accuracy of the QCM). The major problem with TPD as a coverage measuring tool is that it is destructive: the overlayer is fully desorbed in a TPD experiment. As a result, it is used *after* all other measurements have been finished with a particular overlayer film. These may include AES or LEED experiments combined with constant temperature annealing, but care must be taken that the annealing temperatures are kept sufficiently low for desorption not to begin.

Note that in the surface science community the saturation of the high temperature TPD peak is often identified as a coverage of one monolayer. Our data, however, show that on atomically rough surfaces such a simple coverage assignment is not always valid. Only for Pd on the W(211) surface can we clearly distinguish between first and second geometrical monolayers and multilayers. For Pt and Rh on W(211) there is a saturation

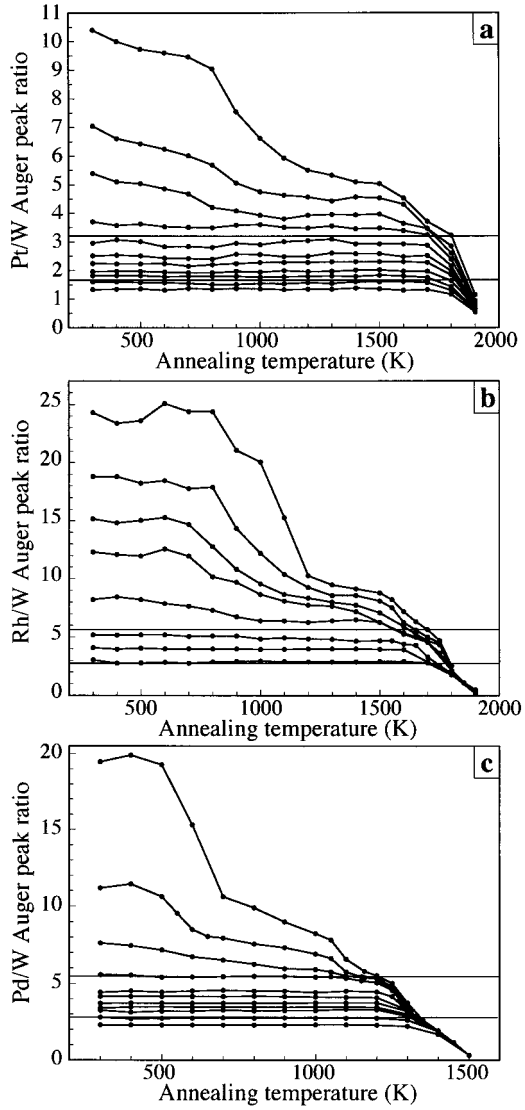

Figure 4. Auger annealing curves for Pt (a), Rh (b), and Pd (c) on W(211), i.e., overlayer to W Auger peak intensity ratio as a function of annealing temperature. Different curves represent different initial coverages. The horizontal lines represent 0.5 and 1 physical monolayer coverages, respectively, as determined by QCM and TPD measurements.

of the high temperature TPD peak at 1 geometrical monolayer but the one physical monolayer (= two geometrical monolayers) peak significantly overlaps with the multilayer desorption curves.

III.b. Auger Annealing Series. The thermal stability of ultrathin metal films on W(211) has been investigated in measurements of Auger annealing curves.[49,50] Metal overlayers are deposited at room temperature and subsequently annealed at temperatures ranging from 400 K up to 1900 K (1500 K for Pd) for 2 min at each temperature. After each annealing, Auger spectra are obtained at room temperature and the differential peak-to-peak amplitudes are measured for overlayer metals and tungsten. The ratio of the Auger peak amplitudes for each overlayer vs W is plotted on Figure 4 (W at 169 eV, Pd at 330 eV, Rh at 302 eV, and Pt at 64 eV). The shape of a particular Auger annealing curve is a function of the initial coverage. On the W(211) surface, for coverages not exceeding one physical monolayer (as calibrated by QCM) the Auger annealing curves remain flat until desorption begins at high temperatures. This indicates that such thin overlayer films are thermally stable on the substrate. In comparison, for coverages in excess of one

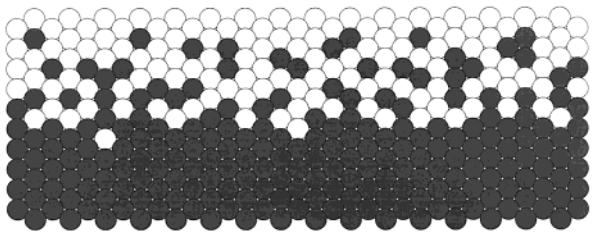

Figure 5. Schematic drawing of the formation of a subsurface alloy phase (side view) Substrate atoms diffuse into the overlayer, while the topmost one physical monolayer of the overlayer remains intact; no substrate atoms are exposed to the surface.

physical monolayer there is a range of temperatures (between 600 and 1000 K) where the overlayer-to-substrate Auger peak ratio decreases. This drop in the overlayer-to-substrate Auger peak ratio has been interpreted in the past as being due primarily to the clustering of the overlayer metal. In accordance with this interpretation, upon dosing at room temperature, the overlayer material forms a uniformly thin layer on the surface due to low surface mobility. However, during annealing, overlayer atoms gain mobility, whereas the first physical monolayer remains flat and completely wets the surface, excess overlayer atoms form three-dimensional clusters. Material inside these three-dimensional clusters is less visible to Auger spectroscopy (the escape depth for Auger electrons in the 50−200 eV energy range is ∼5 Å). After this agglomeration, the Auger curve reaches a plateau until desorption begins. Such clustering of the overlayer material has been seen experimentally for the Pd/W(111) system, using a scanning tunneling microscope.[51] Furthermore, low energy ion scattering (LEIS) measurements[52] show that if the coverage exceeds one physical monolayer the substrate remains fully covered with the overlayer metal (i.e., no W atoms are exposed to the surface) after annealing.

Recent soft X-ray photoelectron spectroscopy (SXPS) measurements for Pt, Pd, Rh, and Ir on W(211) (performed using a synchrotron radiation source),[53,54] however, reveal that at the annealing temperatures, where a drop in the overlayer/tungsten Auger peak ratio is observed, a new alloy phase appears. This phase is interpreted not as adlayer atoms diffusing into tungsten, a process that should be observed for fractional monolayer coverages as well, but as W *diffusing into the overlayer metal* forming a dilute alloy. This is also consistent with Pd−W, Rh−W, and Pt−W bulk alloy phase diagrams;[55] In accordance with these, the solubility of overlayer atoms in a solid W host is very low (∼2 at. %), whereas the solubility of W in the overlayer hosts is relatively high (20−60 at. %).

While alloying takes place at the interface, the topmost one physical monolayer of the overlayer material remains intact, and diffusion affects only layers below it[54] (Figure 5). This increased tungsten concentration close to the topmost atomic layers may also be responsible for the change in overlayer to substrate Auger peak ratios. A combined process of clustering and alloy formation (i.e., the formation of alloyed clusters) is also feasible for metals on W(111), and it would explain STM, Auger, LEIS, and SXPS observations. In the case of W(211), there is no indication of cluster formation in SXPS spectra.[54]

When the overlayer coverage is less than one physical monolayer, the Auger peak ratio remains constant until desorption begins, because neither clustering nor alloy formation takes place, as indicated by both low energy ion scattering[52] and SXPS.[53,54] We use this information to verify the Auger peak ratios for the single physical monolayer coverage as measured by the QCM and TPD; every Auger curve belonging to an overlayer coverage below one physical monolayer should remain

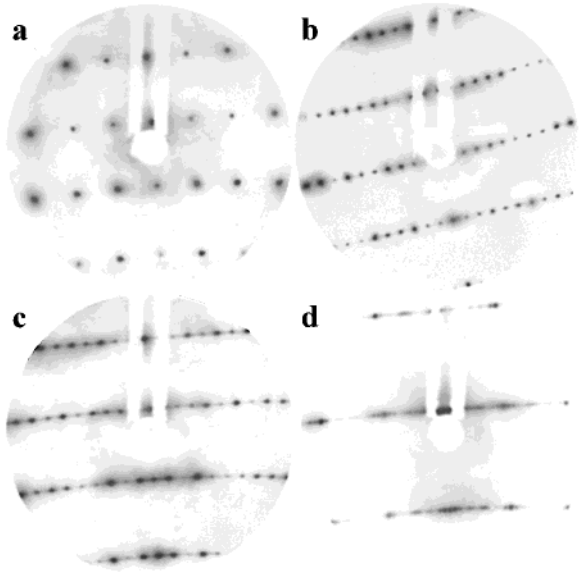

Figure 6. LEED images of the clean and reconstructed W(211) surface. (a) 1×1 pattern from a clean surface, (b) 3×1 reconstruction from a surface covered by ~0.8 physical monolayer of Pt and annealed at 1000 K for 2 min, (c) same 3×1 reconstruction, induced by ~0.8 physical monolayer Rh, also annealed at 1000 K for 2 min, (d) ~0.9 physical monolayer of Pd on W(211), annealed at 900 K for 2 min, the satellite spots are the result of a quasiperiodic (~11×1) reconstruction.

flat, whereas curves belonging to higher overlayer coverages should show a drop in Auger peak intensity ratio. From Figure 4, where the 0.5 and 1 physical monolayer coverages are indicated with horizontal lines for all three overlayers, we can see that the two experiments are indeed in good agreement.

III.c. LEED Results. The clean W(211) surface produces extremely well defined and sharp 1×1 LEED patterns (Figure 6a). When a thin film of Rh, Pt, or Pd is deposited onto the surface, the 1×1 LEED pattern is essentially conserved, with a slight increase in the diffuse background and a decrease in spot sharpness, indicating a slight disorder of the as-deposited overlayer film because of low adsorbate mobility. When annealed to moderate temperatures (400 K), the LEED pattern becomes a sharp 1×1 again, as a pseudomorphic ordering of the film takes place. Although metallic adsorbates in fractional monolayer coverages have been observed to adopt specific superstructures on different tungsten surfaces,[8,12,56,57] we observe no superstructure at room temperature. This is probably because the overlayer materials in question have atomic radii very close to that of tungsten (Pd, 1.38 Å; Pt, 1.39 Å; Rh, 1.35 Å; and W, 1.37 Å), so that they can easily accommodate the atomically rough structure of W(211) perpendicular to the rows and troughs while forming long chains without any specific order along the direction of the troughs.

When annealed to higher temperatures (above 900 K for Rh and Pt, 500 K for Pd) and under certain coverage conditions (as discussed below), LEED shows an $n \times 1$ pattern (n is integer; Figure 6b−d), with the direction of the increased period along [0*1*1], perpendicular to the closed packed atomic rows of the (211) surface (Figure 1). The superstructure is mostly 3×1 for Rh and Pt and ~11×1 for Pd, and in all cases, it is observed only within a certain coverage and temperature range.

This result is very similar to observations made by other groups involving oxygen induced restructuring of the W(211) surface,[31,38] where several different types of $n \times 1$ superstructures were observed as a function of coverage and annealing

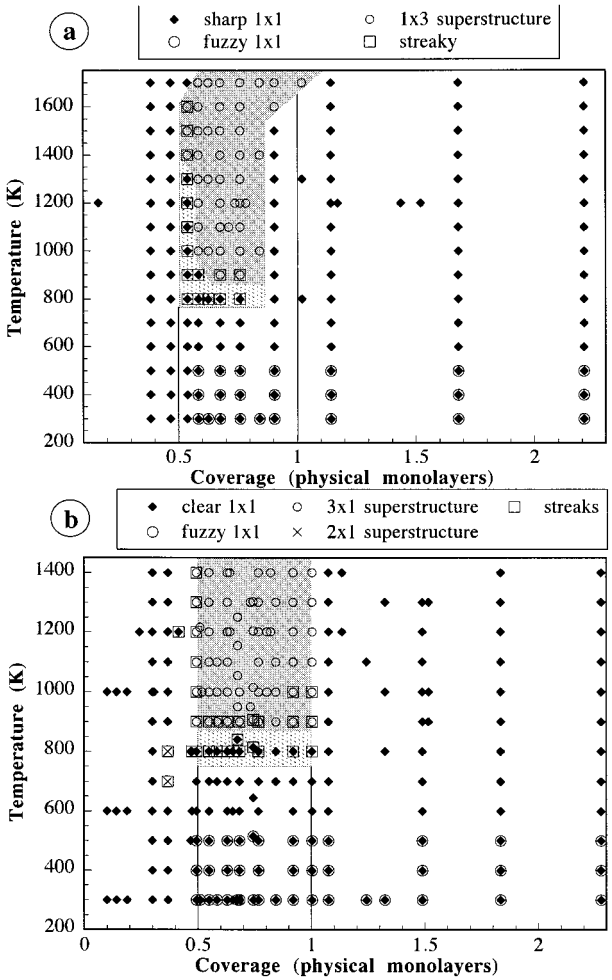

Figure 7. LEED phase diagrams for Pt (a) and Rh (b) on W(211): surface reconstruction as a function of annealing temperature and *initial* overlayer to substrate Auger peak intensity ratio. Coverages of 0.5 and 1 physical monolayer, as measured by a QCM, are indicated.

temperature. The oxygen induced morphology was speculated to be a hill-and-valley type multiple-missing-row reconstruction, essentially microfaceting of the (211) surface into (110) and (101) terraces a few angstroms wide; this is the closest packed surface in a bcc crystal. This explanation is particularly appealing, because such faceting may easily be explained by surface free energy arguments used in the case of the faceting of the W(111) surface. Also, the $n \times 1$ type reconstruction of clean Ir and Pt (110) surfaces via the formation of similar microfacets is a well-established fact.[39−45] These fcc(110) surfaces have row-and-trough structures very similar to that of W(211), and a similar microfaceting is achievable by removing a set of entire rows of atoms from the surface structure.

To determine the coverage and temperature conditions for the superstructure formation, we have performed a set of annealing experiments such as those described before; after each annealing step, LEED is used at room temperature to determine changes in the surface morphology. For Rh and Pt, LEED results are plotted in a phase diagram that shows the type of superstructure as a function of both the initial coverage and the annealing temperature (Figure 7). We have found that the superstructure is limited to a narrow coverage range, between 0.5 and 1 physical monolayer (equivalent to one and two geometrical monolayers on the (211) surface, respectively). The coverage was calibrated using a quartz crystal microbalance,

temperature programmed desorption, and Auger peak intensity ratios as described above.

The surface restructuring process is also kinetically limited as evidenced by the minimum annealing temperature that is needed for the reconstruction to occur. For both Pt and Rh, the temperature threshold is found to be ~900 K. In comparison, the threshold temperature to induce faceting on the overlayer metal/W(111) system is between 700 and 800 K.[28,29]

There is a transition phase bordering the 3×1 superstructure region both for Pt and Rh, where the LEED pattern is very streaky. This indicates a developing disorder in the $[0\bar{1}1]$ direction at the low coverage and low-temperature limits as the surface makes a transition from the 1×1 to the 3×1 structure. The real-space atomic structure of the 3×1 superstructure of Rh/W(211), as observed by STM, is discussed in the following section.

In the case of the Pd covered W(211), the surface undergoes a different kind of restructuring. For a narrow coverage range that falls between 0.5 and 1 physical monolayers, prominent satellites appear on the LEED pattern next to 1×1 diffraction spots (Figure 6d) at temperatures as low as 500 K. These satellites can be interpreted to be caused by a poorly ordered $n \times 1$ superstructure; the spacing between main LEED spots and satellite spots indicates that n is approximately 11. Furthermore, the satellites are always observed along the direction that corresponds to the $[0\bar{1}1]$ direction on the surface, perpendicular to close packed rows, the same as for LEED patterns of the Rh and Pt/W(211) systems. We interpret this observation to be a result of some quasiperiodic superstructure that repeats every n rows, where n will vary in the neighborhood of ~11 in a random fashion.

The restructuring of the Pd/W(211) system appears to have the same kinetic constraints as the Pt and Rh/W(211) systems: the phenomenon is limited to a very narrow coverage range between 0.5 and 1 physical monolayer and requires a minimum annealing temperature. This threshold temperature, however, is much lower in this case; the satellites have been observed at temperatures as low as 500 K. This low temperature threshold indicates that there may be a fundamental difference between the two types of superstructure. The Pd/W(211) superstructure is expected to be entirely due to the periodic rearrangement of the overlayer Pd film, whereas the tungsten substrate is left intact. For the Rh/W(211) and Pt/W(211) systems, on the other hand, it is the substrate itself that undergoes a morphological transformation.

III.d. STM Results. As described above, results from LEED experiments suggested that the Pd, Rh, or Pt covered W(211) surface undergoes a restructuring upon annealing, which manifests itself in various $n \times 1$ LEED patterns. The superstructures observed on Pt/W(211) and Rh/W(211) are predominantly 3×1, whereas the Pd/W(211) superstructure corresponds to ~11×1. The superstructure pattern in both cases is limited to the coverage range between 0.5 and 1 physical monolayers.

Based on structures proposed for the O/W(211) system,[31,38] one possible interpretation of our results is that the 3×1 pattern is due to a hill-and-valley type microfaceting, essentially a triple missing-row type of reconstruction (Figure 8b). One argument in favor of this type of reconstruction is that the microfacets have {110} type orientations, which is expected to be the energetically most stable surface.[35] Although the same microfacted structure is expected for the Rh overlayer induced 3×1 superstructure of W(211), STM scans instead reveal long bands, two atoms wide, covering large terraces of the surface (Figure 9). The bands are parallel to the closed packed rows of the (211) surface (i.e., the [*1*11] direction); they correspond to a double-row, missing row type structure (Figure 8 parts c and d). Occasionally, bands of three or even four closed pack rows are observable (Figure 9 parts c and d).

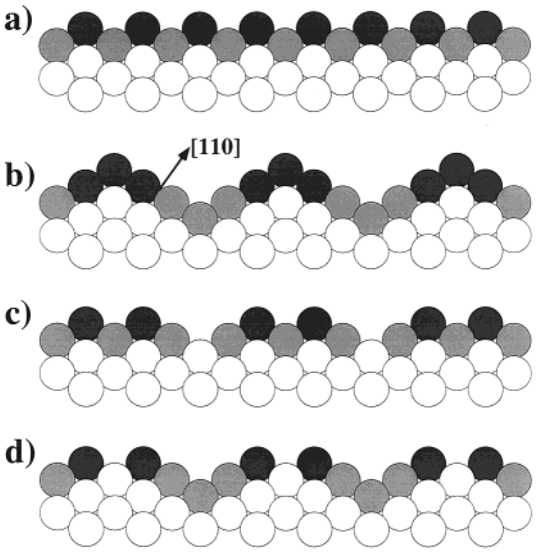

Figure 8. Ball models of possible adsorbate induced surface structures for W(211) (side view). For explanation, see text.

The terraces themselves are bounded by steps that range in height from a single to several geometrical monolayers, and they are arranged in a fish-scale like pattern (Figure 9 parts a and b). At terrace edges where the step height is one geometrical monolayer, the center of a double band on the top terrace is in general aligned with a missing row of the bottom terrace (Figure 9 parts c and d). It is also interesting to note that some of the double-row bands reach far (>100 Å) into neighboring terraces (Figures 9a and 10d), indicating that this double row structure is energetically very stable.

Similar ribbon like structures have been observed for many other systems. These include adsorbates forming long chains from one to a few atoms wide (e.g., Gd on W(110)[58]), a missing row-type reconstruction of the substrate itself as induced by various adsorbates (e.g., O on Rh(110),[59] alkali metals on Ag(110),[60] or K on Cu(110)[5] and Au(110)[61]), and the formation of, sometimes truncated, microfacets (e.g., Au on Pd(110)[6] or vacuum annealed Ir(110)[44]).

For the exact structure within the Rh/W(211) reconstruction, (i.e., the elemental identity of atoms within the structure), we suggest two possible interpretations to our STM data. The first is a 3×1 superstructure in the Rh overlayer (Figure 8c), where the flat W(211) surface is almost fully covered with Rh except for periodic missing rows. This type of reconstruction does not involve any displacement of the tungsten atoms; the W(211) surface is a rigid substrate for the periodic rearrangement of the Rh atoms only.

The second interpretation involves truncated microfacets of W(211), as illustrated in Figure 8d. Note that Figure 8d is identical to the microfaceting model postulated earlier for the oxygen induced reconstruction of W(211) (Figure 8b), except for the missing apex Rh atoms. This scenario is more similar to the faceting of W(111) as induced by Pt, Rh, etc.[28,29] where tungsten atoms are displaced to form the new surface morphology, whereas the surface is covered (almost) uniformly with a thin film of the overlayer. The truncation of sharp features has also been seen for the Pd/W(111) system, where the edges of pyramids are rounded by the removal of apex atoms.[51]

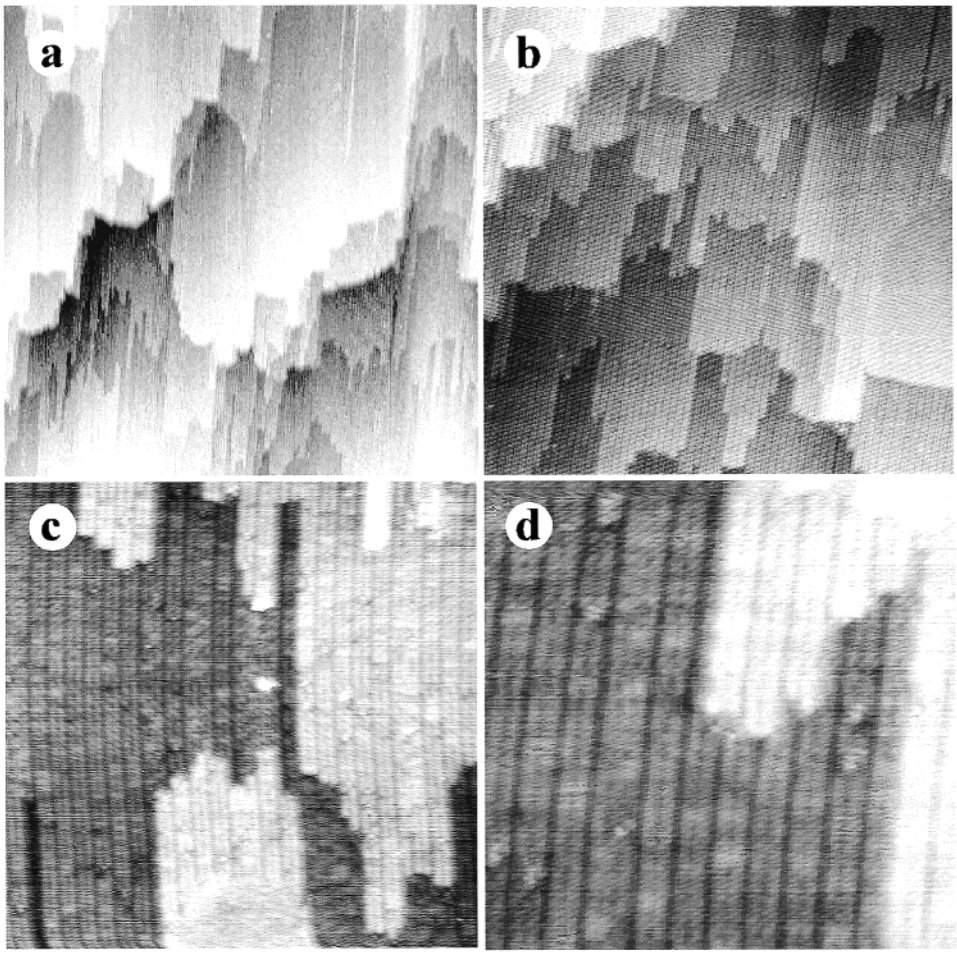

Figure 9. STM scans of ~0.85 physical monolayer of Rh on W(211) annealed at 1200 K. (a) and (b) show the fishscale terrace structure at 2000 and 750 Å, respectively. (c) and (d) reveal the atomic details of the 3×1 superstructure with double-row bands along the $[\bar{1}11]$ direction, parallel with the original row and trough structure of the W(211) surface. Dimensions for scans c and d are 300 and 150 Å, respectively.

Note that both configurations correspond to the same *local* Rh coverage ($^5/_6 = 0.83$ physical monolayers), and there are pro and counter arguments for both models. The best argument for the first model (Figure 8c) is its simplicity. It allows a straightforward explanation as to why the observed superstructure is observed between 0.5 and 1 physical monolayer coverages; as the first geometrical monolayer of Rh atoms is deposited ($\leq$0.5 physical monolayers on the (211) surface), they are randomly distributed in troughs on the substrate, without forming any special superstructure, and the observed LEED pattern is 1×1. As the second geometrical monolayer of Rh is being deposited (between 0.5 and 1 physical monolayers), it assumes a periodic superstructure. Between $^1/_2$ and $^4/_6$ physical monolayers the Rh first fills every third row; between $^4/_6$ and $^5/_6$ monolayers the overlayer begins forming the double row structure of Figure 8c; finally, between $^5/_6$ and 1 physical monolayer Rh atoms start to fill the missing rows between the bands, until the surface is fully covered and flat (Figure 8a). Rh atoms beyond the first physical monolayer coverage do not form any superstructure; hence, the 1×1 LEED pattern returns.

Overlayer superstructures for submonolayer coverages have been observed before for many metallic adsorbate/substrate systems, in particular, Ag, Au, and Ni on the (211) surface of tungsten,[8,56] as well as many other metallic adsorbates on other tungsten surfaces of different orientations.[12,16,27,57,62−65] Such observations are most often explained in terms of adsorbate/substrate atomic size differences and surface stress relaxation. These results would naturally lead us to believe that the 3×1 reconstruction observed on Rh/W(211) and Pt/W(211) are also due to overlayer superstructure formation. However, the atomic radii in our case are not very different (see above) and would certainly not explain the difference we find between Pd/W(211) and the other two systems.

Although the first explanation is much simpler, it also appears to be inconsistent with the observation that background gases from the chamber are always found to adsorb on top of the double rows, rather than in between. STM scans on Figure 10 are from a W(211) sample with 3×1 superstructure, after it has been exposed to background gases in the vacuum chamber for ~3 days. The new bright features on these scans are believed to be adsorbed gas atoms or molecules. Note that background gases always adsorb on top of double rows, rather than in between. This is a very important observation because it is our experience that the overlayer covered tungsten surface is chemically relatively inert, whereas the exposed tungsten is more active. The fact that background gas molecules adsorb on top of the double rows clearly supports the microfaceting model (Figure 8d).

The Rh coverage on the W(211) surface of Figure 10 is very close to one full physical monolayer and demonstrates that, while most of the surface shows the double row structure, there are large patches without any observable corrugation (arrows on Figure 10d). We believe that these patches are due to Rh in excess of $^5/_6$ physical monolayer; these areas are fully Rh covered W(211) surfaces with 1×1 structure (as supported by the very limited amount of observed gas contamination).

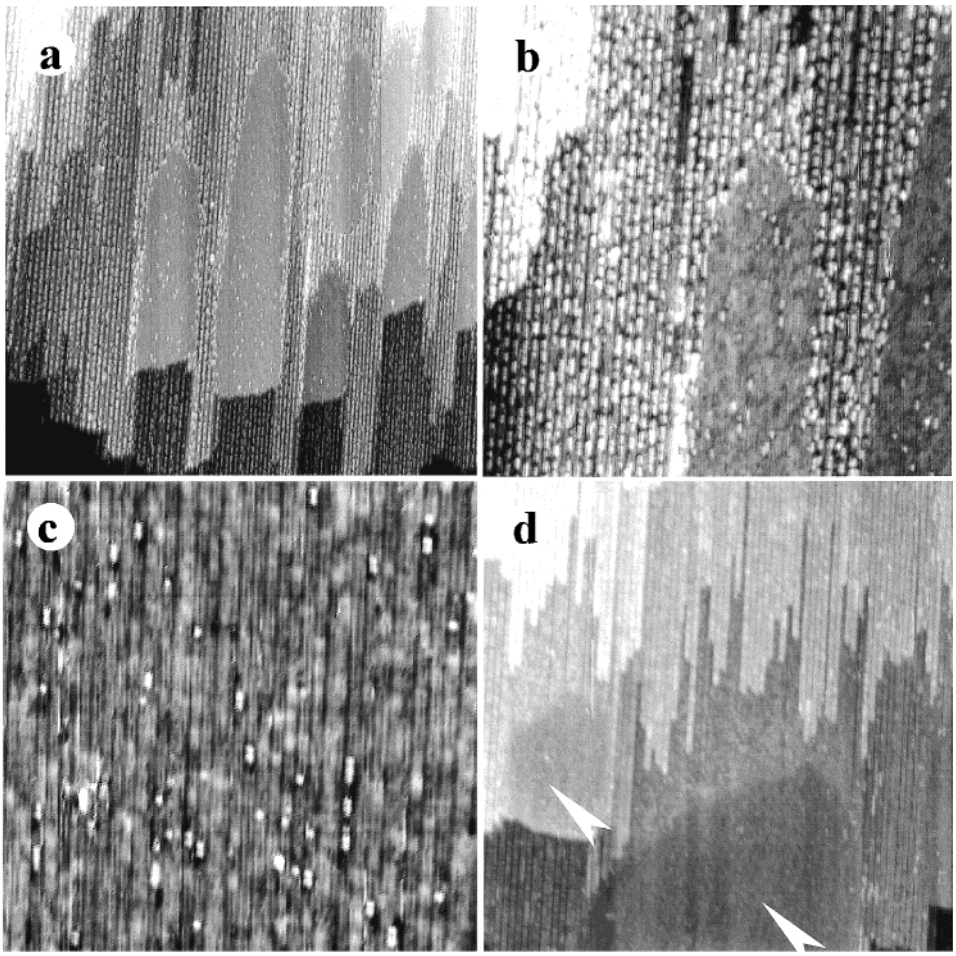

Figure 10. STM images (a−c) are scans of the 3 × 1 superstructure on Rh/W(211) after adsorption of background gases on the surface. Scan dimensions are 1000, 500, and 250 Å, respectively. (d) is a scan (800 Å) of the same surface before gas adsorption, with arrows pointing at large planar regions, where the coverage is assumed to be a full physical monolayer.

On the basis of these observations, our hypothesis is that when the surface is only partially covered ($\sim^5/_6$ physical ML) the energetically favored structure is a microfaceted one as in Figure 8d, stabilized by the Rh overlayer. When the coverage exceeds $^5/_6$ physical monolayer, however, and islands of a full physical monolayer thickness start to form, the planar morphology (Figure 8a) becomes more energetically favorable within the island, rather than the fully microfaceted surface of Figure 8b. Such an extremely coverage-sensitive morphological transition has been reported before for the Pt/W(111) system, where the (111) surface abruptly starts to form facets within isolated islands when the local overlayer coverage reaches one physical monolayer.[66,67]

The two explanations, the one that is based on a superstructure in the Rh film and the other based on the microfaceting of the tungsten substrate, are equivalent except in one respect: that gas adsorption is always observed on top of the double rows. Although simplicity favors the former model, background gas adsorption experiments support the latter, i.e., the microfaceting of the W substrate.

One final argument in favor of the second explanation involves the observation that double rows are stable enough to extend up to 100 Å into neighboring terraces. If the explanation for the 3 × 1 superstructure involves microfaceting of the W(211) surface into a hill-and-valley structure with sides composed of long narrow strips of {011} faces, then the explanation for the stability of such long fringes is the formation of even larger {011} facets (Figure 11). Note that the alignment

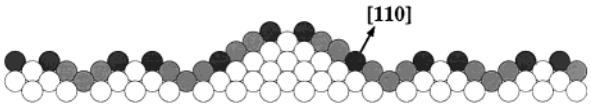

Figure 11. One possible model to explain the stability of single bands extending hundreds of angstroms into neighboring terraces. Such bands would have relatively large {110} surfaces, the closest packed orientation on a bcc surface. This particular example shows the cross section of a band that protrudes 1.5 physical monolayers above the surface.

of the on-top double row fringe with the underlying substrate is also consistent with our STM observations.

Several tests may help in deciding between the two models. One would be to compare the total surface free energy from theoretical, preferably first principles, calculations. A collaboration with the groups of C. T. Chan and T. C. Leung is under way. These groups have already performed many first principles calculations concerning the faceting of W(111) and Mo(111) substrates as induced by metal overlayers.[36,68,69] The initial results of their calculations for the Rh/W(211) system suggests that the microfaceted structure (Figure 8d) is energetically favorable in comparison with the simple reconstruction of Figure 8c.[70] A second test would be a careful structural study based on LEED (I, V) measurements and a structural calculation or a determination of the surface structure using medium energy ion scattering (MEIS).

Finally, as discussed in section III.c, LEED results for the Pd/W(211) system show an $n \times 1$ diffraction pattern for a

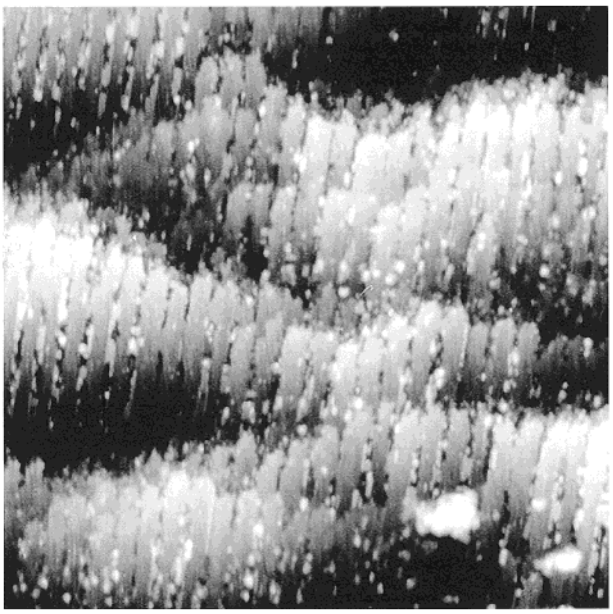

Figure 12. STM scan of ~0.8 ML of Pd on W(211), annealed at ~1000 K (1000 Å × 1000 Å). Dark vertical lines are believed to be missing rows of Pd atoms. Bright spots decorating the missing rows are attributed to adsorbed gases.

narrow coverage range that falls between 0.5 and 1 physical monolayers, upon annealing to temperature above 500 K. The $n \times 1$ diffraction pattern is very poorly defined (Figure 6d), and therefore, it is interpreted as the consequence of a somewhat disordered $n \times 1$ superstructure, where n is ~11. The superstructure is observed along the $[0\bar{1}1]$ direction, perpendicular to close packed rows, the same as for the Rh and Pt/W(211) systems. STM scans of the Pd/W(211) system (Figure 12) suggests that the tungsten surface is atomically flat and is uniformly covered with Pd, except for a quasiperiodic structure of missing rows (dark vertical lines). The average separation between missing rows is approximately 50 Å, which would give rise to an $\sim 11 \times 1$ superstructure, but the missing rows are very much jagged, and the exact separation between missing rows is scattered between 30 and 70 Å. The $\sim 11 \times 1$ superstructure explains the existence of the satellites observed in LEED, whereas the large scatter of the missing row separation accounts for the fact that only those reconstruction spots are observed that are closest to main diffraction spots. Note that on Figure 12, the bright spots that decorate the dark vertical lines of missing Pd rows are attributed to adsorbed background gases, similarly to the Rh/W(211) system on Figure 10.

IV. Summary and Discussion

Rh, Pt, and Pd are found to cause a reconstruction of the W(211) surface similar to oxygen,[31,38] although these bimetallic systems are limited to mostly a 3×1 (Rh and Pt) and $\sim 11 \times 1$ reconstruction (Pd), whereas oxygen has been observed to induce a wide range of $n \times 1$ reconstructions. The oxygen induced morphology was speculated to be a hill and valley type multiple missing row reconstruction,[31,38] essentially microfaceting of the (211) surface into (110) and (101) terraces a few angstroms wide. This explanation is particularly appealing, because such faceting may easily be explained using surface free energy arguments; although faceting increases the total surface area, the surface free energy of the oxygen covered {110} planes is so much lower than that of the (211) that faceting becomes thermodynamically favorable. In fact, a similar argument is applied to the overlayer induced faceting of W(111) into pyramids with sides of {211} orientations,[28] and the lowering of the total surface free energy by faceting has been theoretically verified for a number of overlayer/W(111) and Mo-(111) systems.[36,68,69]

STM experiments, however, do not equivocally confirm the existence of microfacets for these systems. In the case of the Pd/W(211) system, we conclude that the superstructure is entirely due to the rearrangement of the Pd overlayer only: the tungsten surface is uniformly covered with Pd, except for a quasi periodic structure of missing rows. In the case of the Rh/W(211) system, we have presented two possible explanations for the observed 3×1 structure: either the formation of a 3×1 superstructure within the overlayer film that does not affect the underlying W substrate or the formation of a microfaceted structure of the W the substrate, covered with a monolayer film of Rh, truncated at the apex of the resulting ridges. This is similar to the postulated structure for the oxygen induced reconstruction of W(211), but the width of the {110} facets is limited to ~8 Å. We believe that experimental data involving background gas adsorption on the reconstructed surface favors the second explanation: microfaceting of the underlying W substrate.

For all three systems, we have found that there is a narrow coverage range where the reconstruction occurs. In case of the faceting of the metal/W(111) system, a minimum coverage threshold is also found; a high coverage limit, however, has not been observed for that system. LEED and STM observations for both the Pt/W(111)[71] and Pd/W(111)[72] systems suggest that overlayer material in excess of one monolayer does not influence the faceting. Excess material forms clusters (of possible overlayer/tungsten alloys), whereas the rest of the surface is uniformly covered with a single physical monolayer of metal and is fully faceted. On the W(211) surface, however, overlayer material in excess of one physical monolayer does not appear to form clusters, but an overlayer−substrate alloy is formed instead[53,54] (as discussed in section III.b).

One of the most intriguing aspects of the microfaceting reconstruction of Rh/W(211) and Pt/W(211) is the significant amount of mass transport involved in creating the new surface structure. The physical process responsible for the mass transport is surface diffusion of W atoms. The self-diffusion of tungsten has been investigated in great detail using field ion microscopy (FIM).[73−76] It was established that W atoms diffuse readily along the troughs of a W(211) surface, with a diffusion activation energy of ~0.75 eV, whereas cross-channel diffusion has almost never been observed.[75,76] Correspondingly, W adatom diffusion is observable on W(211) below room temperature (~270 K). These observations also suggest that the overlayer induced reconstruction of W(211) is more likely to involve the diffusion of adatoms along the troughs of the surface, than diffusion across the rows. However, to create the microfaceted surface structure of Figure 8d, entire rows of atoms must be displaced within a single terrace. The diffusion probably proceeds across step edges, transporting atoms from one terrace to a neighboring one. This mechanism would also explain the alignment of double-row bands between terraces (cf. Figure 9 parts c and d), such that a truncated apex on one terrace is aligned with a missing row of the neighboring terrace. In our experiments, we established a temperature threshold of ~900 K for the microfaceting to take place, much higher than ~270 K, the temperature threshold for W self-diffusion on the W(211) surface as observed by FIM. The displacement of a large number of W row atoms to relatively long distances (the average terrace width

is on the order of 100 Å), however, may require higher temperatures to proceed in a short time scale (our annealing times are ~2 min).

It must be pointed out, however, that results of FIM measurements of single-atom diffusion on field evaporated surfaces may not be directly relevant to our observations. First, the FIM measurements involved the diffusion of single tungsten atoms (or small clusters) on *clean* tungsten surfaces, whereas our surfaces are covered with at least a physical monolayer of overlayer atoms. Second, FIM samples the random walk of adatoms without the presence of a driving force (such as the lowering of the total surface free energy). Finally, FIM single-atom diffusion experiments on tungsten are conducted at low temperatures, between 270 and 600 K. At the temperatures where well developed facets can be observed on W(111), or the reconstruction of W(211) takes place (>900 K), the surface is disordered and rough,[10] which may make the diffusion proceed at speeds different from expected. In addition, strong intermixing with the overlayer atoms may open up more favorable diffusion pathways (e.g., some type of exchange migration mechanism).

Acknowledgment. The authors acknowledge valuable correspondence and discussions with Dr. C. T. Chan. This work has been supported, in part, by the U.S. Department of Energy, Office of Basic Energy Sciences.

References and Notes

(1) Beauvais, S. L.; Behm, R. J.; Chang, S.-L.; King, T. S.; Olson, C. G.; Rape, P. R.; Thiel, P. A. *Surf. Sci.* **1987**, *189/190*, 1069−1075.
(2) Prince, K. C. *Surf. Sci.* **1988**, *193*, L24-L28.
(3) Clendening, W. D.; Campbell, C. T. *J. Chem. Phys.* **1989**, *90*, 6656−6663.
(4) Leung, W.-Y.; Schmitz, P. J.; Kang, H. C.; Thiel, P. A. *Surf. Sci.* **1991**, *257*, 79−85.
(5) Schuster, R.; Barth, J. V.; Ertl, G.; Behm, R. J. *Surf. Sci. Lett.* **1991**, *247*, L229−L234.
(6) Schmitz, P. J.; Leung, W.-Y.; Kang, H. C.; Thiel, P. A. *Phys. Rev. B* **1991**, *43*, 8834−8840.
(7) Schmitz, P. J.; Leung, W.-Y.; Kang, H. C.; Thiel, P. A. *Phys. Rev. B* **1991**, *44*, 13734−13739.
(8) Kolaczkiewicz, J.; Bauer, E. *Surf. Sci.* **1984**, *144*, 495−511.
(9) Graham, G. W.; Schmitz, P. J.; Thiel, P. A. *Phys. Rev. B* **1990**, *41*, 3353−3359.
(10) Cetronio, A.; Jones, J. P. *Surf. Sci.* **1973**, *40*, 227−248.
(11) Song, K.-J.; Demmin, R. A.; Dong, C.; Garfunkel, E.; Madey, T. E. *Surf. Sci.* **1990**, *227*, L79−85.
(12) Kolaczkiewicz, J.; Bauer, E. *Surf. Sci.* **1999**, *420*, 157−173.
(13) Linsebigler, A.; Lu, G.; Yates, J. T., Jr. *Surf. Sci.* **1993**, *294*, 284−296.
(14) Steigerwald, D. A.; Jacob, I.; Egelhoff, W. F., Jr. *Surf. Sci.* **1988**, *202*, 472−492.
(15) Kief, M. T.; Egelhoff, W. F., Jr. *Phys. Rev. B* **1993**, *47*, 10785−10814.
(16) Schlenk, W.; Bauer, E. *Surf. Sci.* **1980**, *93*, 9−32.
(17) Kolaczkiewicz, J.; Bauer, E. *Surf. Sci.* **1996**, *366*, 71−84.
(18) Schmitz, P. J.; Leung, W.-Y.; Graham, G. W.; Thiel, P. A. *Phys. Rev. B* **1989**, *40*, 11477−11487.
(19) Chang, S.-L.; Wen, J.-M.; Thiel, P. A.; Gunther, S.; Meyer, J. A.; Behm, R. J. *Phys. Rev. B* **1996**, *53*, 13747−13752.
(20) Peebles, H. C.; Beck, D. D.; White, J. M.; Campbell, C. T. *Surf. Sci.* **1985**, *150*, 120−142.
(21) Tikhov, M.; Bauer, E. *Surf. Sci.* **1990**, *232*, 73−91.
(22) Kief, M. T.; Egelhoff, W. F., Jr. *J. Vac. Sci. Technol. A* **1993**, *11*, 1661−1666.
(23) Egelhoff, W. F., Jr. *J. Vac. Sci. Technol. A* **1982**, *20*, 668−670.
(24) Egelhoff, W. F., Jr. *Appl. Surf. Sci.* **1982**, *11−12*, 761−767.
(25) Campbell, R. A.; Rodriguez, J. A.; Goodman, D. W. *Surf. Sci.* **1990**, *240*, 71−80.
(26) Rodriguez, J. A.; Campbell, R. A.; Goodman, D. W. *Surf. Sci.* **1994**, *307−309*, 377−383.
(27) Womeester, H.; Huger, E.; Bauer, E. *Phys. Rev. B* **1998**, *57*, 10120−10131.
(28) Madey, T. E.; Guan, J.; Nien, C.-H.; Dong, C.-Z.; Tao, H.-S.; Campbell, R. A. *Surf. Rev. Lett.* **1996**, *3*, 1315−1328.
(29) Guan, J.; Campbell, R. A.; Madey, T. E. *Surf. Sci.* **1995**, *341*, 311−327.
(30) Madey, T. E.; Nien, C. H.; Pelhos, K.; Kolodziej, J. J.; Abdelrehim, I. M.; Tao, H. S. *Surf. Sci.* **1999**, *438*, 191.
(31) Tracy, J. C.; Blakely, J. M. *Surf. Sci.* **1968**, *13*, 313.
(32) Taylor, N. J. *Surf. Sci.* **1964**, *2*, 544−552.
(33) Zhang, C.; Gellman, A. J.; Farias, M. H.; Somorjai, G. A. *Mater. Res. Bull.* **1985**, *20*, 1129−1135.
(34) Zhang, C.; van Hove, M. A.; Somorjai, G. A. *Surf. Sci.* **1985**, *149*, 326−340.
(35) Chen, S. P. *Surf. Sci.* **1992**, *274*, L619−626.
(36) Che, J. G.; Chan, C. T.; Kuo, C. H.; Leung, T. C. *Phys. Rev. Lett.* **1997**, *79*, 4230−4233.
(37) Guan, J.; Campbell, R. A.; Madey, T. E. *J. Vac. Sci. Technol. A* **1995**, *13*, 1484−1488.
(38) Chang, C. C.; Germer, L. H. *Surf. Sci.* **1967**, *8*, 115−129.
(39) Bu, H.; Shi, M.; Masson, F.; Rabalais, J. W. *Surf. Sci. Lett.* **1990**, *230*, L140-L146.
(40) Stock, M.; Risse, J.; Korte, U.; Meyer-Emsen, G. *Surf. Sci. Lett.* **1990**, *233*, L243−L248.
(41) Koch, R.; Borbonus, M.; Haase, O.; Reider, K. H. *Phys. Rev. Lett.* **1991**, *67*, 3416−3419.
(42) Hetterich, W.; Niehus, H.; Heiland, W. *Surf. Sci. Lett.* **1992**, *264*, L177−L180.
(43) Avrin, W. F.; Merrill, R. P. *Surf. Sci.* **1992**, *274*, 231−251.
(44) Kuntze, J.; Bomermann, J.; Rauch, T.; Speller, S.; Heiland, W. *Surf. Sci.* **1997**, *394*, 150−158.
(45) Hanesch, P.; Bertel, E. *Phys. Rev. Lett.* **1997**, *79*, 1523−1526.
(46) Campbell, R. A.; Guan, J.; Madey, T. E. *Catal. Lett.* **1994**, *27*, 273.
(47) Abdelrehim, I. M.; Pelhos, K.; Madey, T. E.; Eng, J., Jr.; Chen, J. G. *J.Mol. Catal. A: Chem.* **1998**, *131*, 107−120.
(48) Abdelrehim, I. M.; Pelhos, K.; Madey, T. E.; Eng, J., Jr.; Chen, J. G. *J. Phys. Chem. B* **1998**, *102*, 9697−9707.
(49) Madey, T. E.; Song, K.-J.; Dong, C.-Z.; Demmin, R. A. *Surf. Sci.* **1991**, *247*, 175−187.
(50) Rhead, G. E. *J. Vac. Sci. Technol.* **1976**, *13*, 603.
(51) Nien, C.-H. Ph.D. Thesis, Rutgers University, 1999.
(52) Dong, C.; Zhang, L.; Diebold, U.; Madey, T. E. *Surf. Sci.* **1995**, *322*, 221−229.
(53) Kolodziej, J.; Pelhos, K.; Abdelrehim, I. M.; Keister, J. W.; Rowe, J. E.; Madey, T. E. *Prog. Surf. Sci.* **1998**, *59*, 117−134.
(54) Kolodziej, J. J.; Madey, T. E.; Keister, J. W.; Rowe, J. E. *Phys. Rev. B* **1999**, *62*, 5150−5162.
(55) Shunk, F. A. *Constitution of binary alloys*; McGraw Hill: New York, 1969.
(56) Kolaczkiewicz, J.; Bauer, E. *Surf. Sci.* **1984**, *144*, 477−494.
(57) Kolaczkiewicz, J.; Bauer, E. *Surf. Sci.* **1994**, *314*, 221−242.
(58) Pascal, R.; Zarnitz, C.; Bode, M.; Wiesendanger, R. *Surf. Sci. Lett.* **1997**, *385*, L990−L996.
(59) Comelli, G.; Dhanak, V. R.; Kiskinova, M.; Prince, K. C.; Rosei, R. *Surf. Sci. Rep.* **1998**, *32*, 165.
(60) Hayden, B. E.; Prince, K. C.; Davie, P. J.; Paolucci, G.; Bradshaw, A. M. *Sol. St. Com.* **1983**, *48*, 325−327.
(61) Flynn-Sanders, D. K.; Jamison, K. D.; Barth, J. V.; Wintterlin, J.; Thiel, P. A.; Ertl, G.; Behm, R. J. *Surf. Sci.* **1991**, *253*, 270−282.
(62) Yang, Y.-W.; Xu, H.; Engel, T. *Surf. Sci.* **1992**, *276*, 341−352.
(63) Bauer, E.; Hoppa, H.; Todd, G.; Bonczek, F. *J. Appl. Phys.* **1974**, *45*, 5164−5175.
(64) Bauer, E.; Hoppa, H.; Todd, G.; Davis, P. R. *J. Appl. Phys.* **1977**, *48*, 3773−3787.
(65) Kolaczkiewicz, J.; Bauer, E. *Phys. Rev. B* **1991**, *44*, 5779−5785.
(66) Pelhos, K.; Hannon, J. B.; Kellogg, G. L.; Madey, T. E. *Surf. Sci.* **1999**, *432*, 115.
(67) Pelhos, K.; Hannon, J. B.; Kellogg, G. L.; Madey, T. E. *Surf. Rev. Lett.* **1999**, *5*, 767.
(68) Che, J. G.; Chan, C. T.; Jian, W.-E.; Leung, T. C. *Phys. Rev. B* **1998**, *57*, 1875−1880.
(69) Nien, C. H.; Madey, T. E.; Tai, Y. W.; Leung, T. C.; Che, J. G.; Chan, C. T. *Phys. Rev. B* **1999**, *59*, 10335.
(70) Chan, C. T.; Leung, T. C. Private communication.
(71) Dong, C. Z.; Shivaprasad, S. M.; Song, K.-J.; Madey, T. E. *J. Chem. Phys.* **1993**, *99*, 9172−9181.
(72) Nien, C.-H.; Madey, T. E. *Surf. Sci.* **1997**, *380*, L527.
(73) Kellogg, G. L. *Surf. Sci. Rep.* **1994**, *21*, 1−88.
(74) Graham, W. R.; Ehrlich, G. *Surf. Sci.* **1974**, *45*, 530−552.
(75) Wang, S. C.; Ehrlich, G. *Surf. Sci.* **1988**, *206*, 451−474.
(76) Bassett, D. W.; Parsley, M. J. *J. Phys. D: Appl. Phys.* **1970**, *3*, 707.